The Abdus Salam
International Centre for Theoretical Physics

United Nations
Educational, Scientific and
Cultural Organization

IAEA
International Atomic Energy Agency

2292-10

School and Conference on Analytical and Computational Astrophysics

14 - 25 November, 2011

Progressive Transformation of a Flux Rope to an ICME

Sergio Dasso
Instituto de Astronomia y Fisica del Espacio, Buenos Aires
Argentina

Solar Phys (2007) 244: 115–137
DOI 10.1007/s11207-007-9034-2

Progressive Transformation of a Flux Rope to an ICME

Comparative Analysis Using the Direct and Fitted Expansion Methods

S. Dasso · M.S. Nakwacki · P. Démoulin · C.H. Mandrini

Received: 23 February 2007 / Accepted: 14 August 2007 / Published online: 19 September 2007

Abstract The solar wind conditions at one astronomical unit (AU) can be strongly disturbed by interplanetary coronal mass ejections (ICMEs). A subset, called magnetic clouds (MCs), is formed by twisted flux ropes that transport an important amount of magnetic flux and helicity, which is released in CMEs. At 1 AU from the Sun, the magnetic structure of MCs is generally modeled by neglecting their expansion during the spacecraft crossing. However, in some cases, MCs present a significant expansion. We present here an analysis of the huge and significantly expanding MC observed by the *Wind* spacecraft during 9 – 10 November 2004. This MC was embedded in an ICME. After determining an approximate orientation for the flux rope using the minimum variance method, we obtain a precise orientation of the cloud axis by relating its front and rear magnetic discontinuities using a direct method. This method takes into account the conservation of the azimuthal magnetic flux between the inbound and outbound branches and is valid for a finite impact parameter (*i.e.*, not necessarily a small distance between the spacecraft trajectory and the cloud axis). The MC is also studied using dynamic models with isotropic expansion. We have found $(6.2 \pm 1.5) \times 10^{20}$ Mx for the axial flux and $(78 \pm 18) \times 10^{20}$ Mx for the azimuthal flux. Moreover, using the direct method, we find that the ICME is formed by a flux rope (MC) followed by an extended coherent magnetic region. These observations are interpreted by considering the existence of a previously larger flux rope, which partially reconnected with its environment in the front. We estimate that the reconnection process started close to the Sun. These findings imply that the ejected flux rope is progressively peeled by reconnection and transformed to the observed ICME (with a remnant flux rope in the front part).

S. Dasso (✉) · M.S. Nakwacki · C.H. Mandrini
Instituto de Astronomía y Física del Espacio, CONICET-UBA, CC. 67, Suc. 28, 1428 Buenos Aires, Argentina
e-mail: sdasso@iafe.uba.ar

S. Dasso
Departamento de Física, Facultad de Ciencias Exactas y Naturales, Universidad de Buenos Aires, 1428 Buenos Aires, Argentina

P. Démoulin
Observatoire de Paris, LESIA, UMR 8109 (CNRS), 92195 Meudon Principal Cedex, France

Keywords Coronal mass ejection: interplanetary · Magnetic fields: interplanetary · Magnetic reconnection: observational signatures · Solar wind: disturbances

1. Introduction

A magnetic configuration, previously in equilibrium in the solar atmosphere, can reach a global instability threshold when the magnetic stress becomes too high. In this case, the plasma is ejected into the interplanetary (IP) medium and is observed as a coronal mass ejection (CME) by solar coronagraphs. This magnetized mass, which can be expelled as fast as a few thousand kilometers per second, is recognized in IP space as an interplanetary CME (ICME; see, *e.g.*, Wimmer-Schweingruber *et al.*, 2006). During its travel from the Sun to 1 AU, fast CMEs are slowed down by drag forces between the ICME and the solar wind environment (see, *e.g.*, Vršnak and Gopalswamy, 2002). Thus, at 1 AU they can reach speeds as high as $\sim$1000 km s^{-1}.

1.1. Magnetic Clouds

Magnetic clouds (MCs) are a particular subset of ICMEs. They are formed by twisted magnetic flux tubes that carry a large amount of magnetic helicity from the Sun to the IP medium. They also transport significant amounts of magnetic flux, mass, and energy. The principal characteristics of these magnetic structures are *i*) an enhanced magnetic field, *ii*) a smooth rotation of the magnetic field vector through a large angle ($\approx$180°), and *iii*) a low proton temperature (Klein and Burlaga, 1982).

The magnetic field in MCs is relatively well modeled by Lundquist's model (Lundquist, 1950), which considers a static and axially symmetric linear force-free magnetic configuration (*e.g.*, Goldstein, 1983; Burlaga, 1988, 1995; Lepping, Burlaga, and Jones, 1990; Lynch *et al.*, 2003). However, many other different models have been also used to describe the magnetic structure of MCs.

Some models consider the MC as a rigid body during the time it travels through the solar wind and crosses the spacecraft. Farrugia *et al.* (1999) considered a cylindrical shape for the cloud cross section and a nonlinear force-free field, whereas Mulligan *et al.* (1999), Hidalgo *et al.* (2002), and Cid *et al.* (2002) considered a cylindrical cloud but a non-force-free field. Noncylindrical static models have been also applied to MCs (*e.g.*, Hu and Sonnerup, 2001; Vandas and Romashets, 2002). A comparison of global quantities (magnetic fluxes and helicity) derived from different static models has been made by Dasso *et al.* (2003) and Dasso *et al.* (2005b). Different techniques have been compared by using synthetic data and analyzing the output of numerical simulations of MCs (Riley *et al.*, 2004).

Some MCs present a significantly larger velocity in their front than in their back, a characteristic of expansion. Thus, some authors have used dynamical models to describe these clouds during the observation time; they have considered two cases: with a radial expansion only (see, *e.g.*, Farrugia *et al.*, 1993; Osherovich, Farrugia, and Burlaga, 1993; Farrugia, Osherovich, and Burlaga, 1997; Nakwacki *et al.*, 2005) and with expansion in both the radial and axial directions (see, *e.g.*, Shimazu and Vandas, 2002; Berdichevsky, Lepping, and Farrugia, 2003). Some dynamical models consider an expanding elliptical shape for the MC (*e.g.*, Hidalgo, 2003). The main aim of these models is to take into account the evolution of the magnetic field as the spacecraft crosses the MC, then, to correct the effect of mixing the spatial variation and time evolution of the observations to get a better determination of the MC field (and related characteristics).

1.2. Aims of this Study

We analyze the MC detected inside the ICME observed at L1 between 9 Nov. 2004, at 20:25 UT and 11 Nov. 2004, at 18:45 UT (Harra *et al.*, 2007). This is a very fast, left-handed and huge MC with a size larger than 0.2 AU in the Earth – Sun direction. It has a very intense magnetic field (>40 nT) and expands strongly, with a velocity of ∼850 km s^{-1} in its front and ∼600 – 700 km s^{-1} in its back, depending on where the rear boundary is set. This MC presents one of the largest (ever observed) velocity differences between its front and back (Nakwacki *et al.*, 2007).

We analyze this MC using a model-independent method, called the direct method (Dasso *et al.*, 2006). It takes into account the magnetic flux conservation in closed structures, such as flux ropes. This method gives us an estimation of the magnetic flux in the MC directly from the data and allows us to improve the determination of the orientation of the MC axis, as well as its boundaries. Finding the boundaries for some MCs is an open issue (Russell and Shinde, 2005; Wimmer-Schweingruber *et al.*, 2006). Indeed, several authors, using different proxies, set them at different times with the consequent differences in the estimated MC axial orientation and in the estimations of global magnetohydrodynamic quantities.

In Section 2, we describe the magnetic and plasma properties of the MC. Then, in Section 3, we present the direct method and the results obtained. In Section 4, we fit the two dynamical models to velocity and magnetic field observations. From the fitted models we compute the magnetic fluxes and compare them with the values obtained from the static Lundquist's model and from the direct method. Finally, in Section 5, we give a summary and our conclusions.

2. The Studied Cloud

In this section we analyze *in situ* magnetic and plasma observations of the MC observed on 9 – 10 Nov. 2004, which is located inside an ICME. We define a local frame of coordinates, attached to the MC, and we analyze the data in this frame.

2.1. One or Two Clouds?

An ICME was observed from 20:25 UT on 9 Nov. to ≈18:45 UT on 11 Nov. The ICME is preceded by typical piled-up solar wind material (panel n_p in Figure 1). This corresponds to plasma and magnetic field pushed from behind by the ICME, forming the turbulent pre-ICME sheath (notice the high level of fluctuations in θ_B). A forward shock is located in front of the sheath (at 9:15 UT on 9 Nov.). This event presents also a nontypical second shock inside the sheath that precedes the ICME (at 18:20 UT on 9 Nov.). For a deeper description of shocks and their association with solar sources see Harra *et al.* (2007), in particular their Table I.

The end of the ICME is marked by a thick solid line (11 Nov. at 18:45 UT; label "end" in Figure 1) as defined by Harra *et al.* (2007). After 11 Nov. at 18:45 UT, the magnetic field is consistent with Parker's spiral (changes of magnetic sectors are observed in ϕ_B). The higher level of magnetic fluctuations, typical of the fast solar wind, confirms this interpretation.

Two MCs were initially reported inside this ICME: the first one starting on 09 Nov. at 20:54 UT and finishing on 10 Nov. at 03:24 UT, and the second one starting on 10 Nov. at 03:36 UT and finishing on 10 Nov. at 11:06 UT (http://lepmfi.gsfc.nasa.gov/mfi/mag_cloud_S1.html). The rotation of the field is indeed larger than usual (close to one turn; Figure 1).

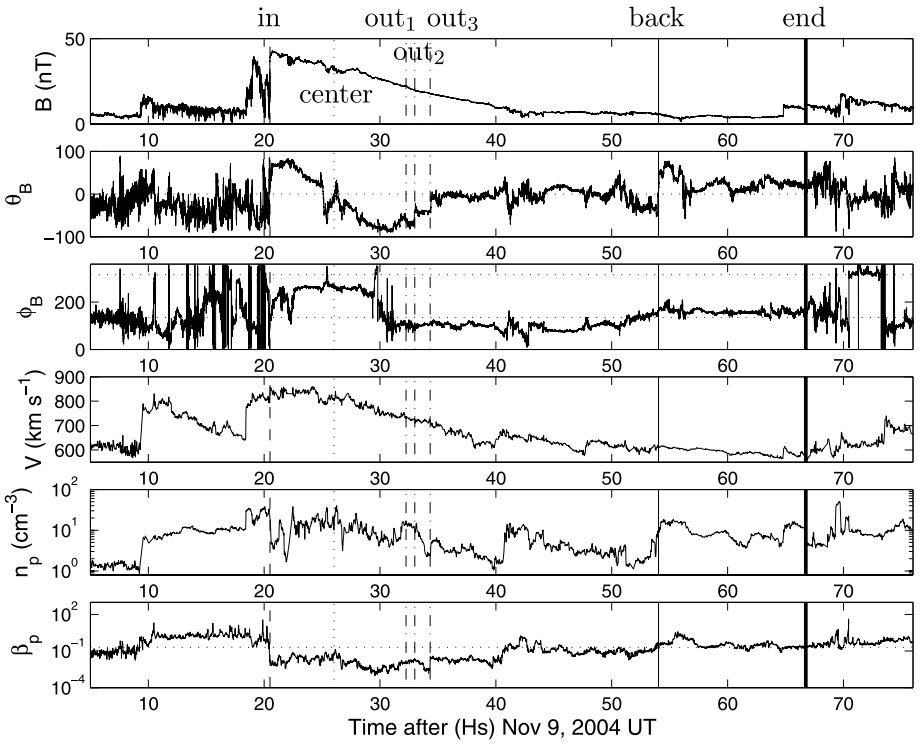

Figure 1 Wind observations for the magnetic cloud observed inside the ICME of 9 – 11 Nov. 2004 (time cadence of 100 s). From upper to lower panels: absolute value of the magnetic field ($B = |\mathbf{B}|$), latitude (θ_B) and longitude (ϕ_B) angles of **B** in GSE coordinates, the bulk velocity (V), the proton density (n_p), and the proton plasma beta (β_p), all as a function of time. The vertical dashed line "in" corresponds to the start of the field's coherent rotation (beginning of the MC on 9 Nov. at 20:30 UT), the vertical dotted line corresponds to the cloud center (10 Nov. at 02:02 UT; see Section 3.3), the vertical dash-dotted lines "out_1" and "out_3" correspond to the extremes of the range of possible endings for the rotation of **B** (end of the cloud on 10 Nov. at 08:15 UT and 10:20 UT), and the dash-dotted line "out_2" corresponds to a strong discontinuity (in between this range, on 10 Nov., at 09:00 UT). The thin solid vertical line "back" marks a strong magnetic discontinuity (11 Nov. at 06:02 UT) and the thick vertical solid line "end" marks the end of the ICME (11 Nov. at 18:45 UT). Horizontal dotted lines in θ_B and ϕ_B panels indicate the orientation of Parker's spiral; the one in the β_p panel marks the mean value for a set of MCs studied by Lepping *et al.* (2003).

Moreover, the magnetic field observed has indeed a nonclassical structure: It is very strong in the front, progressively decreases in the back, and has an extended weak tail. Still, a coherent and continuous variation of both the field strength and the plasma velocity is observed, without clear evidence of two independent magnetic structures.

Other studies concluded that only one extended MC was present. In Harra *et al.* (2007) and Longcope *et al.* (2007) the boundaries of the magnetic cloud were selected as starting on 9 Nov. at 20:30 UT and finishing on 10 Nov. at 10:00 UT. Similar boundaries (starting on 9 Nov. at 20:40 UT and finishing on 10 Nov. at 10:20 UT) were chosen by Qiu *et al.* (2007). Both the direct method and data modeling confirm the presence of only one flux rope (Sections 3 and 4).

2.2. Summary of the Cloud Observations

We analyze the *in situ* measurements of the magnetic field components obtained by the Magnetic Field Instrument (MFI, Lepping *et al.*, 1995) and the plasma quantities obtained by the Solar Wind Experiment (SWE, Ogilvie *et al.*, 1995), both aboard *Wind*. There is a small data gap in SWE on 9 Nov. from 21:58 UT to 22:27 UT (see Figure 1).

The magnetic field observations are in GSE (Geocentric Solar Ecliptic) coordinates. In this right-handed system of coordinates, $\hat{x}_{\rm GSE}$ corresponds to the Earth – Sun direction, $\hat{z}_{\rm GSE}$ points to the North (perpendicular to the ecliptic plane), and $\hat{y}_{\rm GSE}$ is in the ecliptic plane and points to the dusk when an observer is near Earth (thus, opposing to the planetary motion).

The front boundary of the MC (9 Nov. at 20:30 UT) is well defined (vertical dashed line in Figure 1, label "in"). The magnetic field presents a North – West – South rotation with time (see θ_B and ϕ_B panels in Figure 1); thus, the MC is formed by a left-handed flux rope with its axis almost on the ecliptic and pointing to the West ($y_{\rm GSE} < 0$ or $\phi_B \sim 270°$).

A characteristic of this MC is its very strong expansion (see panel V in Figure 1). The observed plasma velocity V goes from $\sim$850 km s^{-1} at the beginning to $\sim$700 km s^{-1} close to the cloud end, a difference of 150 km s^{-1} in the observed time range ($\sim$15 hours). This implies an expansion of $\sim$10 km s^{-1} per hour.

The MC rear boundary is uncertain; the vertical dash-dotted lines in Figure 1 indicate a possible range (from 10 Nov. at 8:15 UT to 10:20 UT, labels "out$_1$" and "out$_3$", respectively). However, the decrease of $|\mathbf{B}|$ and the strong expansion are still present at later times, indicating a backward extension of the MC. The mean value of $\beta_{\rm p}$ (ratio of the proton pressure to the magnetic pressure) is 0.12 for a sample of MCs studied by Lepping *et al.* (2003) (horizontal dotted line in panel $\beta_{\rm p}$ of Figure 1). Then, another indication that the MC is more extended in the back is the presence of $\beta_{\rm p} < 0.12$ after 10:20 UT. This region extends up to a strong discontinuity in θ_B and density (on 11 Nov. at 06:02 UT, labeled "back" in Figure 1). We call the region between "out$_3$" and "back" simply the back region of the MC. Finally, there is a region with weak, but coherent, field between the "back" and "end" boundaries. The physical origin of these regions is analyzed in Section 3.5.

2.3. Orientation and Extension of the Cloud

To facilitate the understanding of the MC properties, we define a system of coordinates linked to the cloud in which $\hat{z}_{\rm cloud}$ is along the cloud axis (with $B_{z,\rm cloud} > 0$). We define the latitude angle (θ) between the ecliptic plane and the cloud axis, as well as the longitude angle (φ) between the projection of the axis on the ecliptic plane and the Earth – Sun direction ($\hat{x}_{\rm GSE}$) measured counterclockwise. Then, when $\theta = 90°$ ($\theta = -90°$) the cloud axis is parallel (antiparallel) to $\hat{z}_{\rm GSE}$ and it points to the ecliptic North (South). When $\theta = 0°$ the cloud axis is on the ecliptic plane, with $\varphi = 0°$ being the case of the axial field pointing toward the Sun, and $\varphi = 90°$ ($\varphi = 270°$) when it points to the terrestrial dusk (dawn).

Because the speed of an MC is nearly in the Sun – Earth direction and is much larger than the spacecraft speed (which can be supposed to be at rest during the cloud observing time), we assume a rectilinear spacecraft trajectory in the cloud frame. The trajectory defines a direction $\hat{d}$ (pointing toward the Sun); then, we define $\hat{y}_{\rm cloud}$ in the direction $\hat{z}_{\rm cloud} \times \hat{d}$ and $\hat{x}_{\rm cloud}$ completes the right-handed orthonormal base ($\hat{x}_{\rm cloud}$, $\hat{y}_{\rm cloud}$, $\hat{z}_{\rm cloud}$). We also define the impact parameter p as the minimum distance from the spacecraft to the cloud axis. Then, we construct a rotation matrix from the GSE system to the cloud system and obtain the components of the observed magnetic field in the cloud coordinates: $B_{x,\rm cloud}$, $B_{y,\rm cloud}$, $B_{z,\rm cloud}$.

The local system of coordinates is especially useful when p is small compared to the MC radius (R). In particular, for $p = 0$ and an MC described by a cylindrical magnetic configuration $\mathbf{B}(r) = B_z(r)\hat{z} + B_\phi(r)\hat{\phi}$, we have $\hat{x}_{\rm cloud} = \hat{r}$ and $\hat{y}_{\rm cloud} = \hat{\phi}$ when the spacecraft leaves the cloud. In this particular case, the magnetic field data will show the following: $B_{x,\rm cloud} = 0$, a large and coherent variation of $B_{y,\rm cloud}$ (with a change of sign), and an intermediate and coherent variation of $B_{z,\rm cloud}$, from low values at one cloud edge, taking the largest value at its axis and returning to low values at the other edge.

The minimum variance (MV) method (Sonnerup and Cahill, 1967) has been used to estimate the orientation of MCs (see, *e.g.*, Bothmer and Schwenn, 1998; Lepping, Burlaga, and Jones, 1990; Farrugia *et al.*, 1999; Dasso *et al.*, 2003; Gulisano *et al.*, 2005). It gives a good estimation if p is small compared to R and if the inbound and outbound magnetic fields are not significantly asymmetric.

However, when the cloud presents a strong expansion, as in the event studied here, the directions derived by the MV method will mix two different effects in the variance of **B**: (1) the effect of the coherent rotation of **B** (which provides the cloud orientation) and (2) the effect of the cloud "aging" (the decrease of the field strength with time as a result of magnetic flux conservation combined with cloud expansion). This latter effect is not associated with the cloud orientation; thus, we apply the MV technique to $\mathbf{B}/|\mathbf{B}|$ to decrease the cloud aging consequences.

We start the analysis taking the "in" and the "out$_3$" boundaries, since the strongest magnetic discontinuity is located at "out$_3$". With these boundaries, we find the typical shape of the components of **B** in the cloud frame, as previously discussed (see Section 3.3 for further justifications). The MV method applied to the normalized field gives $\theta = -23°$ and $\varphi = 274°$. With the same procedure and an end boundary on 10 Nov. at 10:00 UT, Harra *et al.* (2007) found $\theta = -20°$ and $\varphi = 276°$. Changing the cloud end between "out$_1$" and "out$_3$" gives ranges for θ and φ of $\theta \sim [-25°, 0°]$ and $\varphi \sim [260°, 280°]$.

2.4. The Data in the Cloud Frame

Figure 2 shows the components of the magnetic and velocity field in the cloud frame for an orientation of the cloud axis such that $\theta = -10°$ and $\varphi = 275°$ (this orientation is justified in Section 3.2). The magnetic field components show the typical large-scale shape of MCs when the impact parameter is small compared with the cloud radius. However, an inner and nontypical substructure is present at its center (mainly observed in $B_{y,\rm cloud}$, where it is antisymmetric).

A strong expansion is observed in the velocity components, mainly along $\hat{x}_{\rm cloud}$. This is expected from the MC orientation and the data in GSE since, cloud axis oriented such as $\varphi \sim 270°$, the spacecraft cannot observe different parcels of fluid along a large range of $z_{\rm cloud}$ values. However, a weak signature of expansion along the cloud axis can be observed in $V_{z,\rm cloud}$ (Figure 2). For an MC with $\theta \sim 0°$ and $\varphi > 270°$, an axial expansion is characterized by $V_{z,\rm cloud} < 0$ in the front, changing to $V_{z,\rm cloud} > 0$ in the back. This is just what is observed in our case when the mean value of $V_{z,\rm cloud}$ is removed within the cloud. This gives us the clue that φ is larger than 270°.

When the spacecraft crosses a cylindrical MC (or an elliptical one with one of the main axes parallel to the Sun – Earth direction) and $p = 0$, $B_{x,\rm cloud} \approx 0$. The first panel in Figure 2 shows that the observed $B_{x,\rm cloud}$ has a slightly negative mean value. The sign of $B_{x,\rm cloud}$, together with the evolution of $B_{y,\rm cloud}$, implies that the flux rope axis is above the ecliptic plane.

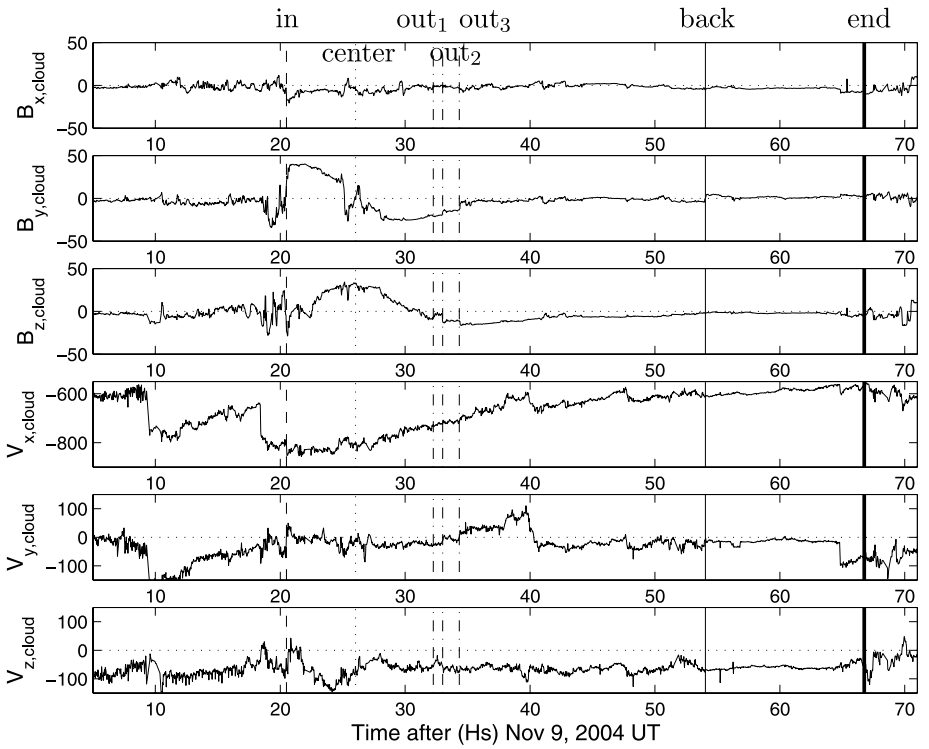

Figure 2 From upper to lower panels, observed magnetic and velocity field components in the cloud frame. In this frame $\hat{z}_{\text{cloud}}$ is along the cloud axis ($\theta = -10^{\circ}$ and $\varphi = 275^{\circ}$ in GSE coordinates), $\hat{y}_{\text{cloud}}$ is orthogonal to both the MC axis and the spacecraft trajectory, and $\hat{x}_{\text{cloud}}$ completes the right-handed orthogonal base. Vertical lines correspond to the same times as in Figure 1. The region between "in" and "center" is called the inbound region and those between "center" and "out_1" or "out_2" or "out_3" are the outbound regions. From "out_1" or "out_2" or "out_3" up to "back" we have the back region; after that and up to "end" completes the ICME extension.

3. Results with the Direct Method

3.1. The Direct Method

In this section we summarize and extend the direct method presented by Dasso *et al.* (2006). This method lets us find the rear boundary of a flux rope for a given axis orientation, or the reverse, the MC orientation for a given position of the rear boundary. The front boundary of a flux rope is usually well defined by a discontinuity of the magnetic field (changing abruptly from a fluctuating field in the MC sheath to a strong and coherent field within the MC). The corresponding current sheet is expected to be present all around the flux rope as the limit between magnetic regions with different magnetic connectivities and so with different magnetic stresses. A corresponding magnetic discontinuity, labeled "out", is then expected at the rear of the MC. The flux rope is present in between these two discontinuities and the same amount of azimuthal flux is traversed twice by the spacecraft.

Let us consider a flux rope at a given time. The conservation of the magnetic flux ($\nabla \cdot \mathbf{B} = 0$) across a plane formed by the spacecraft trajectory and $\hat{z}_{\rm cloud}$ (with $y_{\rm cloud}$ constant) gives

$$\int_{\rm flux\ rope} B_{y,\rm cloud}\, {\rm d}x\, {\rm d}z = 0, \tag{1}$$

with x and z being the spatial coordinates in the $\hat{x}_{\rm cloud}$ and $\hat{z}_{\rm cloud}$ directions, respectively (Dasso *et al.*, 2006).

The observations provide only $B_{y,\rm cloud}$ as a function of time along the trajectory. So, we need two hypotheses: an invariance of $B_{y,\rm cloud}$ along the flux rope axis and the conservation of the magnetic flux with time. The first hypothesis is justified by a low ratio of the MC radius over the expected curvature radius of the axis and the balance of magnetic torques, which is expected to homogenize the field along the axial direction (Dasso *et al.*, 2006). The second hypothesis is valid as long as the amount of magnetic flux reconnected during the spacecraft crossing is low. Indeed, we have found that magnetic flux is reconnected in the front of the MC (see Section 3.5). An estimation of the amount of flux reconnected during the spacecraft crossing gives ∼5% of the initial azimuthal flux (see Section 3.6); so, unless the reconnection rate is much higher during the observing time than it was during the travel from the Sun, the amount of reconnected flux is small during the crossing. In the following we neglect such reconnected flux.

The elementary flux crossed during ${\rm d}t$ is $B_{y,\rm cloud}(t) L(t) V_{x,\rm cloud}(t)\, {\rm d}t$, where $L(t)$ is the axial length of the portion of the flux rope that had a length $L_{\rm in} = L(t_{\rm in})$ when the spacecraft entered the MC. Then, Equation (1) becomes

$$\int_{\rm flux\ rope} B_{y,\rm cloud}(t) L(t) V_{x,\rm cloud}(t)\, {\rm d}t = 0. \tag{2}$$

If the axis orientation and the position of one boundary of an MC are known, this flux balance property can be used to find the MC center and the other boundary as follows. We define the accumulative flux per unit length as

$$\frac{F_y(x)}{L_{\rm in}} = \int_{t_{\rm in}}^{t(x)} B_{y,\rm cloud}(t') \frac{L(t')}{L_{\rm in}} V_{x,\rm cloud}(t')\, {\rm d}t', \tag{3}$$

where $t_{\rm in}$ is the time of the MC front boundary (located at $x = X_{\rm in}$) and $x = \int_{t_{\rm in}}^{t} V_{x,\rm cloud}(t')\, {\rm d}t'$. The position where $F_y(x)/L_{\rm in}$ has its absolute extreme gives an estimation of the position where the spacecraft reaches the closest distance to the MC axis. This indicates the x position of the MC center; this estimation is more precise when the impact parameter is lower. Then, when $F_y(x)/L_{\rm in}$ goes back to zero at $x = X_{\rm out}$, we have the other boundary. The region from $x = X_{\rm in}$ to $x = X_{\rm out}$ defines the MC flux rope.

Since the ratio of the MC radius to the Sun distance is small (typically ≈0.1 or lower), $L(t')/L_{\rm in} \approx 1$. In the following we derive a correction to this estimation. If the MC axis does not change its shape drastically and if it does not disconnect from the Sun during the crossing time, its length evolves proportionally to its distance from the Sun, $D(t)$, so $L(t)/L_{\rm in} = D(t)/D_{\rm in}$ (where $D_{\rm in} \approx 1$ AU for the present observations). Moreover, the cloud's global velocity, which is the velocity of its center, $V_{\rm c}$, is not expected to change significantly during the crossing time; then, we have

$$\frac{L(t)}{L_{\rm in}} \approx \frac{D(t)}{D_{\rm in}} = 1 + (t - t_{\rm in}) \frac{V_{\rm c}}{D_{\rm in}}. \tag{4}$$

All terms in the right-hand side of Equation (3) can be derived from observations.

3.2. Refined Orientation of the Cloud

The direct method was previously applied to the 18 – 20 Oct. 1995, MC (Dasso *et al.*, 2006). The orientation of its axis was well determined. The strong frontal discontinuity in the magnetic field was naturally related to another strong backward discontinuity, the flux balance given by Equation (2) was satisfied, and $L(t)$ was constant.

The orientation of the axis of the MC studied here is not so well determined; then, we explore different orientations to find which angles (θ and φ) give a cancellation of F_y at the strongest magnetic discontinuity observed at the MC rear (labeled "out$_3$" in Figures 1 and 2), at the inner extreme labeled "out$_1$", and at the intermediate time "out$_2$" (between "out$_1$" and "out$_3$"). Because of the orientation of the MC (*i.e.*, its axis almost lying on the ecliptic and perpendicular to the Sun – Earth direction) F_y is mostly affected by the value of θ. We find $\theta = -10^\circ \pm 10^\circ$ from variations of the end boundaries in the full range between "out$_1$" and "out$_3$" and using the two extreme possibilities on the axial expansion [no axial expansion, $L(t) = L_{\rm in}$, and axial expansion proportional to the distance to the Sun, Equation (4)]. The value of φ is constrained by imposing that $B_{x,\rm cloud}(t)$ should have a small variation with time (as expected in flux rope models) and so gives no contribution to azimuthal or axial field components. This gives $\varphi = 275^\circ \pm 10^\circ$.

The left panel of Figure 3 shows F_y for $L(t) = L_{\rm in}$ (no axial expansion) and an orientation such that F_y is canceled at the discontinuity "out$_3$", which gives $\theta = -10^\circ$ and $\varphi = 275^\circ$. The rear boundary of the MC is in fact ambiguous from the data, since there is also a strong discontinuity between "out$_1$" and "out$_3$" ("out$_2$" on 10 Nov. at 09:00 UT); see Figures 1 and 2. Fixing the previous orientation, but using the axial expansion given in Equation (4) (see right panel of Figure 3), we find that the cancelation of F_y is now at "out$_2$". With this boundary, we find a much less extended region with a reversal of $B_{z,\rm cloud}$ at the back of the MC. So, this boundary gives an MC field closer to the one inferred from a classical MC model. In this case, the results of the direct method agree with those of the fitted models (including expansion; Section 4). These is evidence that we have identified the right end boundary and orientation of the flux rope.

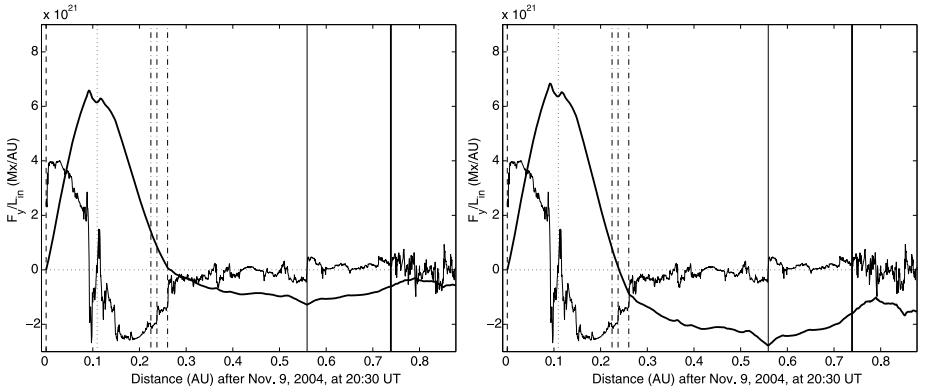

Figure 3 Component of **B** perpendicular to both the trajectory of the spacecraft and to the cloud axis ($B_{y,\rm cloud}$, thin curve) and accumulated magnetic flux of this component per unit length ($F_y/L_{\rm in}$, thick curve). The dotted vertical line marks the cloud center (10 Nov. at 02:02 UT). Left and right panels correspond to computation of $F_y/L_{\rm in}$ without [$L(t) = L_{\rm in}$] and with axial expansion [Equation (4)], respectively. In both panels the cloud orientation was taken as $\theta = -10^\circ$ and $\varphi = 275^\circ$. The vertical lines indicate the same positions as in Figures 1 and 2.

3.3. Structure of the Cloud

The field component $B_{y,\mathrm{cloud}}$ vanishes at three locations near the cloud center (close to the vertical dotted line at the abscissa ∼0.1 AU in Figure 3). Taking into account the expected antisymmetry of the inbound and outbound regions, we set the cloud center at 10 Nov. at 02:02 UT (dotted line in Figure 3). Then, the accumulated flux F_y/L_{in} [Equation (3)] gives a unique relationship between the inbound and outbound data, since it labels each flux surface. This relationship is better shown using F_y/L_{in} in the abscissa and reversing the sign of $B_{y,\mathrm{cloud}}$ inside the outbound branch (Figure 4). Then, peaks and valleys of $B_{y,\mathrm{cloud}}$ in the inbound and outbound branches can be related. As expected, this association is stronger near the MC center where the regions that are crossed are closer and also more isolated from the interaction with the solar wind environment (Dasso *et al.*, 2005a). Except for the strong discontinuity at the MC borders, the association between structures is not clear outside the core (where $B_{y,\mathrm{cloud}}$ has no characteristic variations that can be recognized in both the inbound and outbound branches).

There is a clearly distinguishable substructure in the cloud center seen as reversed peaks in $B_{y,\mathrm{cloud}}$ and as a valley in F_y/L_{in} (Figure 3). It has a small extension, $\sim \pm 10^{-2}$ AU, and is globally antisymmetric. A less evident substructure was also present in the previously analyzed MC (18 Oct. 1995; Dasso *et al.*, 2006).

If $p = 0$, the central substructure would imply the presence of a small twisted flux tube with opposite magnetic helicity in the center of the flux rope. The formation of such a structure is not possible in the corona. An analysis of several possibilities indicates that the simplest interpretation is the following: close to the minimum approach, the spacecraft trajectory is nearly tangent to the magnetic flux surfaces of the flux rope ($B_{y,\mathrm{cloud}} \approx 0$). Any warping of the flux surfaces gives a clear signal in the $B_{y,\mathrm{cloud}}$ component. For geometrical reasons, such warping is more difficult to detect outside the center (where $B_{y,\mathrm{cloud}}$ is important). It is noteworthy that such structure will be evident only if the magnetic data are rotated to the correct MC frame to have no mixing with the strong $B_{z,\mathrm{cloud}}$ component.

For the 18 Oct. MC, the warping was moderate and $B_{y,\mathrm{cloud}}$ kept its sign inside both the inbound and the outbound regions. For the 9 – 10 Nov. MC, the warping is more marked, as sketched in Figure 5. This figure shows (to the right) a scheme of the spacecraft trajectory

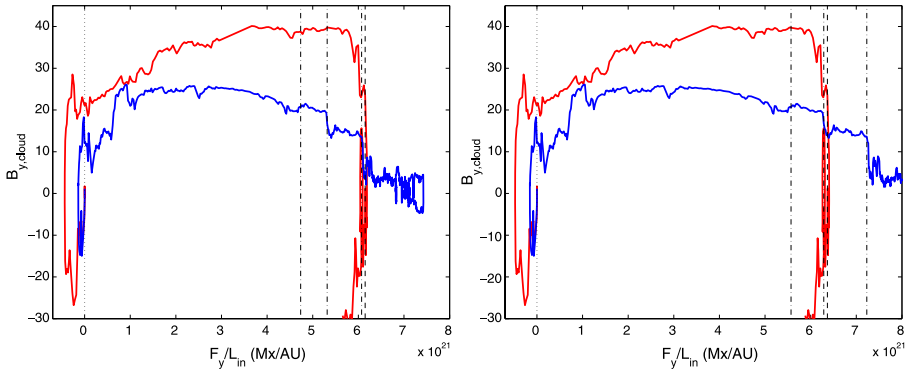

Figure 4 Inbound (red) and outbound (blue) y_{cloud} component of **B** as a function of the accumulated magnetic flux of this component per unit length (F_y/L_{in}). F_y/L_{in} is computed as in Figure 3. The difference in the amplitude of $B_{y,\mathrm{cloud}}$ between the inbound and outbound regions is due to the MC aging (not corrected here).

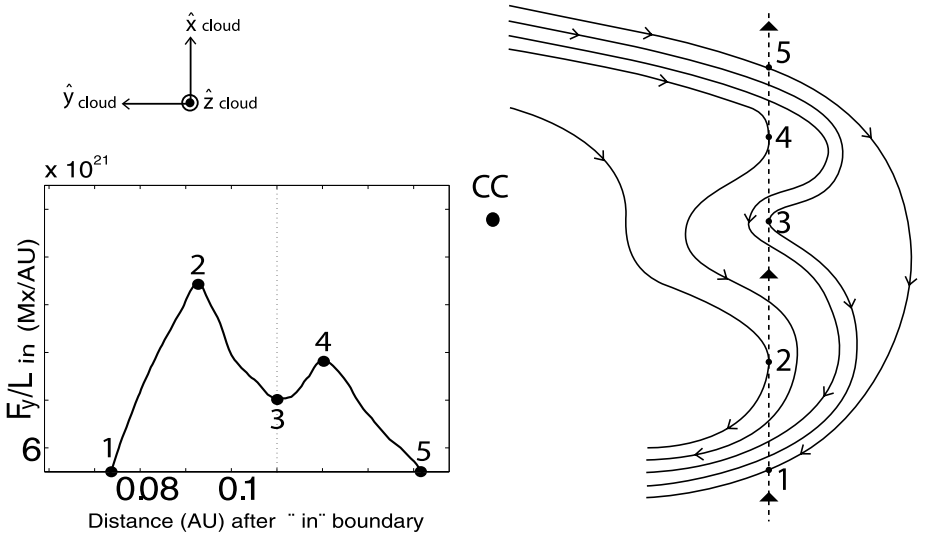

Figure 5 Scheme of the magnetic field lines near the MC central region (right) and the corresponding $F_y/L_{\rm in}$ evolution along the spacecraft trajectory (inset, a zoomed version of Figure 3). The magnetic structure of the flux rope is undulated, probably because of its fast evolution and interaction with the surrounding medium. The undulations are amplified in this scheme for clarity, but in the observed MC they are significant enough to produce reversals of $B_{y,\rm cloud}$. The dot marked CC indicates the location of the cloud center. Numbers 1, 2, 3, 4, and 5 are reference points of the observed field lines.

(vertical dashed line) across the MC core field lines (solid warped lines). The core crossing starts at field line 1 and ends at 5. The large dot labeled CC marks the cloud center position. It is located toward positive values of $y_{\rm cloud}$ since the cloud axis is above the ecliptic plane (see the last paragraph of Section 2.4). If one considers the cloud as a flux rope, which is compatible with the observations, the same accumulated flux $F_y/L_{\rm in}$ implies that the inbound and outbound field lines are connected (*i.e.*, they are in fact the same field line observed twice). Thus, for example, 1 is connected to 5. The flux $F_y/L_{\rm in}$ has a local maximum at 2 and 4 and a local minimum at 3 when the spacecraft trajectory is tangent to the field lines.

3.4. Magnetic Fluxes

The total azimuthal flux F_ϕ is estimated by taking $F_y(x_{\rm center})$ and assuming that $p = 0$. The largest source of uncertainty is the length of the flux rope, $L_{\rm in}$, and in a more general way the assumed invariance by translation. Since this cloud presents signatures of being detached at one of its legs (Harra *et al.*, 2007), we assume an initial length $L_{\rm in} = 1.5$ AU, an intermediate value of those used in previous papers. The uncertainty in the MC boundary of the outbound branch has a lower effect because the difference of F_ϕ found with the boundary "out$_1$" and "out$_3$" is only about 10% (see Table 1).

The axial flux F_z, across a surface perpendicular to the cloud axis, can be estimated directly from the observations by assuming a circular MC cross section, $p = 0$, and neglecting the expansion to compute $r = x(t) - x_{\rm center}$. Here, we neglect the axial flux in the core since it is a correction of the order of $(p/R)^2$; see Dasso *et al.* (2006). Then, for the outbound

branch we compute F_z^{outbound} as

$$F_z^{\text{outbound}} = 2\pi \int_{t_{\text{center}}}^{t_{\text{out}}} B_{z,\text{cloud}}(t')\big[x(t') - x_{\text{center}}\big] V_{x,\text{cloud}}(t')\, \mathrm{d}t'. \tag{5}$$

(A similar expression holds for F_z^{inbound}, but with the integration between t_{center} and t_{in}.) As in previously studied MCs (*e.g.*, Mandrini *et al.* 2005, 2007; Attrill *et al.*, 2006) F_z is one order of magnitude lower than F_ϕ (see Table 1).

3.5. Structure of the ICME

The analysis of F_y/L_{in} in Section 3.3 indicates that this MC is not a simple flux rope. Some of the MC characteristics (see Figure 1), such as an unusually high magnetic field with a low variance, a low β_{p}, and a strong expansion, continue well after the rear boundary of the flux rope ("out$_1$", "out$_2$", and "out$_3$"). We discuss in the following the most plausible physical scenario to create such magnetic structure.

There is an extended region where $B_{y,\text{cloud}}$ still has a negative and coherent behavior from position "out$_3$" to "back", so the accumulated flux keeps increasing monotonically (Figure 3). This behavior was also found in the 18 – 20 Oct. 1995, MC and it was interpreted as the remnant of an originally larger magnetic flux rope whose front was partially reconnected with the overtaken magnetic flux, as shown in Figure 6 of Dasso *et al.* (2006). In the example analyzed here, this interpretation has even more support from the data, since part of the overtaken flux is still present in front of the MC and we can estimate when reconnection started.

There is a coherent negative $B_{y,\text{cloud}}$ field just in front of the MC (from ≈18:00 UT to 20:30 UT; Figure 2). We interpret this as the remnant of the magnetic flux that reconnected with the original flux rope. At the time of observations, the MC overtakes this structure with a velocity difference of ≈40 km s^{-1}; so reconnection is driven. Such a velocity difference is crucial for reconnection efficiency because its rate increases with a larger velocity difference (Schmidt and Cargill, 2003). Furthermore, Burlaga (1995) and Farrugia *et al.* (2001) have found that magnetic holes, such as the one preceding the MC analyzed here (top panel of Figure 1), are associated with magnetic reconnection.

Taking into account the previous reconnection scenario, the back region, where $B_{y,\text{cloud}}$ still has a coherent negative value, is simply the magnetic flux at the periphery of the original flux rope. This back region keeps the properties of typical MCs without fitting in the standard flux rope models. If the front reconnected, this back region would be connected to the solar wind field; so, the magnetic field direction can change because of the propagation of Alfvén waves, as observed here with the reversal of $B_{z,\text{cloud}}$ (Figure 2). However, if there is no other reconnection process, the flux of $B_{y,\text{cloud}}$ cannot be removed from the back of the MC; in fact, we find no other field to allow such reconnection. Thus, the closed (flux-balanced) flux rope observed at 1 AU is embedded in a larger structure, which includes an extended back region. This flux rope was part of a larger one that was partially peeled at its front because it reconnected with its environment.

3.6. Clues for Magnetic Reconnection

The high velocity of the MC ($V_{\text{c}} \approx 800$ km s^{-1}), compared to its surroundings (≈600 km s^{-1}) implies a progressive extension of the back region (between boundaries "out$_3$" and "back" in Figure 2). Assuming that the relative velocity, $V_{\text{c}} - V_{\text{back}}$, was similar at earlier times

and that the $B_{y,\mathrm{cloud}}$ component (in the back region) had initially a value similar to that in the rear of the MC (because of pressure balance), we can estimate the period of time δt between the start of reconnection and the MC observations. The range of time between the observation of the two extremes of the expanding region (between "out$_3$" and "back") is $\tau_{\mathrm{expansion}} \approx 18$ hours. This corresponds to a spatial extension of $\sim \tau_{\mathrm{expansion}} V_{\mathrm{back}}$ when the region was observed. So, the back region expands in size by $\tau_{\mathrm{expansion}} V_{\mathrm{back}}$ since the start of reconnection at the MC front. This extension has its origin in the relative velocity between the MC and the back region (which becomes lower because of its magnetic connection to the solar wind). From the beginning of the reconnection at the MC front, starting a lapse of time δt earlier than the observations, the "back" boundary progressively separates from the MC with a relative velocity $V_{\mathrm{MC}} - V_{\mathrm{back}}$. Assuming that this relative velocity was not changing drastically during the MC transit, the back region expanded by $\approx (V_{\mathrm{MC}} - V_{\mathrm{back}})\delta t$. Equating the previous estimations of the back region extension, we find

$$\delta t \approx \frac{\tau_{\mathrm{expansion}} V_{\mathrm{back}}}{V_{\mathrm{c}} - V_{\mathrm{back}}} \approx 18 \times 600/200 \approx 54 \text{ hours}. \tag{6}$$

The solar event that is the most probable source for the MC studied here occurred in AR 10696. It is a multiple event that starts with a steep rise in GOES light curve at ∼15:50 UT on 7 Nov. and has two clear peaks, one at ∼16:00 UT and the other at ∼16:35 UT. At the time of the second peak a large two-ribbon flare was observed within AR 10696, but also two Hα ribbons were seen at both sides of an erupting transequatorial filament extending from AR 10696 to AR 10695 at the southwest (see Harra *et al.*, 2007). During this intense event that reached class X2.0 in soft X rays the full neutral line, which formed a switchback, erupted. The CME observed in the Large Angle and Spectroscopic Coronagraph (SOHO/LASCO) C2 on 7 Nov. at 16:54 UT is associated with this multiple flare involving AR 10696 and the erupting transequatorial filament to the southwest. Longcope *et al.* (2007) have proposed that the source of the MC is the AR eruption, but Harra *et al.* (2007) have considered both possibilities: either the AR or the transequatorial filament eruption. We discuss these scenarios in view of our IP analysis.

Taking ∼15:50 UT on 7 Nov. as the start time of the solar event, and taking an arrival time for the MC front at ∼20:30 UT on 9 Nov., we obtain a transit time of ∼52 hours, comparable to the transit time (∼47 hours) computed assuming a constant MC velocity of -800 km s^{-1} and the spacecraft located at L1. Both estimations are comparable to δt [Equation (6)]; this implies that reconnection started when the flux rope was close to the Sun.

What could be the magnetic structure present in front of the flux rope, probably already from its origin in the corona? The field in front of the MC is oriented mostly southward with an average field intensity of ~ -30 nT, though there is a structure of northward oriented field with a temporal length between 19:54 UT and 20:01 UT on 9 Nov., an average field strength of ~ -15 nT, and a spatial extension of ∼0.002 AU (if one takes an average velocity of ~ -800 km s^{-1}). Analysis of the MDI magnetogram on 7 Nov. shows that the most probable origin of the southward oriented structure is the large-scale, nearly potential field of AR 10696. If the source of the MC is the AR eruption, then the core of the AR should become kink unstable (see Williams *et al.*, 2005, who analyzed an eruption that occurred three days later in the same AR). In the kink instability, part of the twist is transformed into writhe, implying a strong rotation of the axis of the flux rope. Taking into account the MC orientation found in Section 3.2 gives a rotation of ∼160°. The MHD simulation of Gibson *et al.* (2004) gives a writhing of the flux tube of ∼120° (before it reconnects with the overlying field). Numerical simulations by Török and Kliem (2005) confirm this using a different approach and, indeed, the writhing could be as large as a rotation of 160° depending on the properties

of the overlying field (T. Török, private communication). So the amount of rotation and its direction (for a left-handed flux rope), if the MC flux rope comes from the AR, is coherent with recent MHD simulations of kink-unstable flux ropes.

Interplanetary scintillation observations suggest that the material from the core of the AR was ejected primarily northward and, thus, it could remain unobserved at 1 AU (see Harra *et al.*, 2007). In this scenario, and if the source of the MC is the trans-equatorial filament eruption, the direction of the trans-equatorial filament and the cloud axis differ by 67° (see Figure 12 in Harra *et al.*, 2007). Moreover, the sense of rotation from the filament to the cloud axis is opposite to the one expected from the development of a kink instability in a region of left-handed magnetic helicity. As discussed by Harra *et al.* (2007), it may happen that the kink instability has not played a role far away from the strong fields of the AR. The northward oriented structure observed between 19:54 UT and 20:01 UT on 9 Nov. could be related to the northward oriented trans-equatorial loops observed above the filament. However, in both scenarios reconnection should be forced between the ejected flux rope and the AR arcade field from the beginning of the eruption. This explains the origin of a nearly antiparallel field (if one neglects the short period of northward directed field) in front of the flux rope from the beginning of the launch, as indicated by a value of δt similar to the transit time.

Our previous discussion has implications for the reconnection rate in a collisionless plasma. While the erupting flux rope pushed against an overlying nearly antiparallel magnetic field, we still observe part of this overlying flux in front of the MC at 1 AU! Of course we have no way to determine how the strength of the forcing nor the time dependence of the reconnection rate during the flux rope transit. Still this observation is a clue that magnetic reconnection is not efficient in a collisionless plasma, as expected from classical theory. Some recent observations show direct evidence of magnetic reconnection in a collisionless plasma such as the solar wind (Gosling *et al.*, 2005). Some numerical simulations show that the Hall effect can increase the reconnection rate above the classical rate (*e.g.*, Morales, Dasso, and Gómez, 2005). Our observations set a constraint on the reconnection rate, which can be quantified only after a numerical modeling of the flux rope ejection and transit to 1 AU.

From the computed accumulated flux (Figure 3) we can estimate the relative amount of reconnected flux from the original flux rope ejected from the Sun as $\approx 1.25/7.4 \approx 17\%$, assuming $L(t) = L_{\rm in}$ (left panel). With the expansion length given by Equation (4), the flux present in the back part, which is the fraction of reconnected flux, is $\approx 30\%$ [although it is not obvious that we can use Equation (4) for the back part where the field is connected to the solar wind]. The relative amount of flux present in front of the MC is $\approx 0.6/7.4 \approx 8\%$. This implies that the relative amount of stable (not kinked), archlike magnetic flux above the erupting flux rope is between 25% and 38% of the azimuthal flux in the MC.

Finally, a fraction of the $B_{y,\rm cloud}$ magnetic flux observed after the boundary "in" is expected to be reconnected when the spacecraft exits the flux rope. To estimate an order of magnitude for this flux, let us suppose that the reconnection rate was comparable to its mean value during the transit from the Sun. The amount of reconnected flux during the MC observing time is the ratio of the crossing time ($\approx$14 hours) over the transit time from the Sun ($\approx$52 hours) times the flux reconnected from the Sun. Then, $\sim$5% of the original flux was reconnected during the MC crossing time. So, the fraction of flux reconnected between $t = t_{\rm in}$ and $t_{\rm out}$ is expected to be an amount much lower than the uncertainties in the flux estimations (see Table 1).

4. Results Using Fitted Models

This cloud presents a large velocity difference between its front and rear parts (fourth panel in Figure 1). This velocity difference is the consequence of a large MC size and a significant expansion. Both conditions imply that the magnetic field is observed at significantly different times during the MC crossing and thus at times when the MC has significantly different sizes. As a consequence of magnetic flux conservation, this implies the observed decay of B with time (upper panel of Figure 1). Then, $B_{z,\mathrm{cloud}}$ and even more so $B_{y,\mathrm{cloud}}$ (since it is stronger close to the flux rope borders) present a remarkable asymmetry between the inbound and outbound branches. Moreover, the center of the cloud is observed before the central observing time for the full structure, as expected for a spatially symmetric expanding object.

In this section we compare the observations to fitted models describing the evolution of the magnetic field assuming an isotropic self-similar expansion. The observed velocity is used to derive the expansion rate, which is then used in the expansion magnetic model. We also quantify the magnetic fluxes from the fitted models and compare them with the results obtained from a classical static model and the direct method.

4.1. Expansion Model

We assume an isotropic self-similar expansion of the MC, where all distances are multiplied by a factor $f(t)$:

$$\mathbf{r}(t) = \mathbf{r}_0 f(t), \tag{7}$$

where $f(t_0) = 1$ and $\mathbf{r}_0$ is the position of a given element of fluid at some reference time t_0. Since the MC front boundary, called "in", is well defined, we select this as the reference time, $t_0 = t_{\mathrm{in}}$. Each element of fluid is labeled by its $\mathbf{r}_0$ value, then the $\mathbf{r}_0$ coordinate is a marker of each element of fluid (Lagrangian coordinates).

We assume in the following that the flux rope size increases linearly with time. Then, $f(t)$ can be written as

$$f(t) = 1 + (t - t_{\mathrm{in}})/T, \tag{8}$$

where T is the time of expansion. If Equation (8) were valid for the entire transit time from the Sun, then the flux rope size would vanish at time $t = t_{\mathrm{in}} - T$, so T would also be approximately the transit time from the Sun to the position observed at t_{in}. In practice, we use Equation (8) only during the MC crossing; so, we are only assuming a local linear increase of the size with time. Depending on the evolution during the transit from the Sun, T could be different from the transit time.

The time evolution for the plasma velocity $\mathbf{V}$ in the cloud frame comes from Equation (7) by taking the temporal derivative and keeping $\mathbf{r}_0$ fixed (thus following a plasma element):

$$\mathbf{V}(t) = \frac{\mathbf{r}}{T + t - t_{\mathrm{in}}} = \frac{\mathbf{r}_0}{T}. \tag{9}$$

The first part of the equation gives the velocity at a given time t, so it is proportional to the distance. The velocity decays with time, but this decay is only apparent since when one follows a given plasma element, defined by $\mathbf{r}_0$, the velocity is in fact constant (second equality). Then, Equation (8) implies that there are no forces acting on any plasma element (free expansion). This is an *a posteriori* justification of Equation (7); for an isotropic expansion, an initial force-free field stays force free.

The observed speed is the sum of the expansion speed and of the global speed of the MC. During the time of observation, we can assume that the MC is globally moving at a constant speed $-V_c$ (velocity of the MC center) along $\hat{x}_{\rm cloud}$ because the aerodynamic drag significantly affects V_c only on a time scale comparable or larger than the transit time to 1 AU. We also assume that the spacecraft is at rest. Then, the velocity component along $\hat{x}_{\rm cloud}$ is

$$V_x = -V_c + V_c \frac{t - t_c}{T + t - t_{\rm in}}. \tag{10}$$

This equation is fitted to the data to derive V_c, t_c (the time when the spacecraft crosses the cloud center), and T. It is noteworthy that the nearly linear observed V_x is a consequence of the constant speed V_c, and not of the linear expansion with time assumed in Equation (8). The assumed expansion introduces only a nonlinear correction in $(t - t_{\rm in})$ because the crossing time, $t_{\rm out} - t_{\rm in}$, of the MC is small compared to the time of expansion, T. [A further correction would come from the nonlinear development of a general $f(t)$]. This justifies the use of Equation (8).

4.2. Results for the Expansion

The observed $V_{x,\rm cloud}$ has a globally linear variation with time within the MC (Figure 6). To better show its variation, we subtract the mean value of the velocity computed inside the range of positions "in" to "out$_3$": $\langle V_{x,\rm cloud}\rangle = -794$ km s^{-1}. When the impact parameter (p/R) is small, as it is in this MC, this speed represents the radial velocity with respect to the cloud axis, such that for a cloud in expansion, $V_{x,\rm cloud} - \langle V_{x,\rm cloud}\rangle$ is negative before the spacecraft reaches the cloud axis and positive after that.

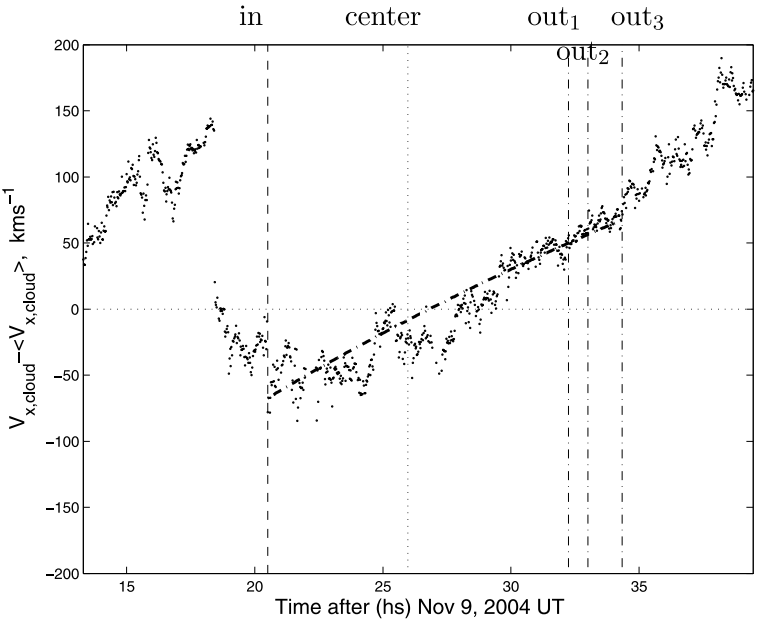

Figure 6 Observed (dots) and fitted (thick dash-dotted line) radial velocity profile ($V_{x,\rm cloud} - \langle V_{x,\rm cloud}\rangle$). Vertical lines mark the same times as in Figure 1.

From a least-square fitting of Equation (10) to the velocity data inside the "in" to "out$_3$" boundaries, we obtain $T \approx T_3 = 73$ hours (≈3 days). We find a slightly longer time of expansion $T \approx T_1 = 79$ hours (≈3.3 days) when the fit is restricted to the interval between the "in" and "out$_1$" boundaries, and we get $T_2 = 77$ hours (≈3.2 days) for boundaries "in" to "out$_2$". Considering the self-similar expansion given by Equation (8) implies that the MC has expanded from the time $t_{\rm in}$ by factors of 1.19 and 1.15 when the spacecraft crossed "out$_3$" and "out$_1$", respectively.

Both times of expansion, T_3 and T_1, are longer than the transit time from the Sun (≈52 hours; Section 3.6). Taking an approximately constant global velocity $V_{\rm c}$, we find that the distance of the MC front to the Sun increases by the factor $D(t)/D_{\rm in} \approx 1+(t-t_{\rm in})V_{\rm c}/D_{\rm in}$ [see Equation (4)]. Doing the ratio of the measured expansion rate variation $[\frac{{\rm d}f(t)}{{\rm d}t}]$ to $\frac{\rm d}{{\rm d}t}[\frac{D(t)}{D_{\rm in}}]$, we obtain a nondimensional factor $D_{\rm in}/(V_{\rm c}T)$. This factor is 0.64 and 0.59 for boundaries "out$_3$" and "out$_1$", respectively. Given the orientation of the MC ($\theta = -10°$ and $\varphi = 275°$), the velocity in Figure 6 is measured mainly across the flux rope. Then, the MC is expanding at a significantly smaller rate radially than what we expect assuming the isotropic expansion in Equation (4).

Assuming that the spacecraft trajectory is close enough to the MC axis, $p/R \ll 1$, we can compute the radius of the flux rope from the observed velocity since the distance crossed $(\int V_{x,\rm cloud}\,{\rm d}t)$ is $R_{\rm in} + R_{\rm out} = R_{\rm in}[1 + f(t_{\rm out})]$. Taking the boundary "out$_3$", we find $R_{\rm in} = 0.12$ AU and $R_{\rm out3} = 0.14$ AU; for boundary "out$_1$" we find smaller radii, $R_{\rm in} = 0.10$ AU and $R_{\rm out1} = 0.12$ AU. If we do not consider the expansion, we get the mean values because the distance crossed is simply $2R$.

4.3. Magnetic Field Models

Lundquist's static model (Lundquist, 1950) is a classical linear force-free configuration ($\nabla \times \mathbf{B} = \alpha \mathbf{B}$, with α constant). From the conservation of the magnetic flux during the expansion, and by assuming a Lundquist's field at a given time, it is possible to derive an expansion field model (see, *e.g.*, Shimazu and Vandas, 2002; Berdichevsky, Lepping, and Farrugia, 2003). We will also consider a more general model where the amplitude of the azimuthal and axial components are independent. This represents an approximation for a flux rope with an oblate cross section (see Vandas and Romashets, 2003, for an exact solution). We consider this modified expansion Lundquist's model to keep the same functional dependence of the field components, so the difference among the three models is only the number of free parameters (and the physics involved).

The three models are described by the equations following:

$$B_r(r,t) = 0, \tag{11}$$

$$B_\phi(r,t) = B_{{\rm in},\phi}\ {\rm f}^{-2}\ J_1(\alpha_{\rm in}\ r/{\rm f}), \tag{12}$$

$$B_z(r,t) = B_{{\rm in},z}\ {\rm f}^{-2}\ J_0(\alpha_{\rm in}\ r/{\rm f}), \tag{13}$$

where $B_{{\rm in},\phi}$, $B_{{\rm in},z}$, and $\alpha_{\rm in}$ are the field and α values when the spacecraft enters the MC at $t = t_{\rm in}$. For the static model ${\rm f} = 1$ and $B_{{\rm in},\phi} = B_{{\rm in},z} = B_{\rm in}$, so there are only two free parameters, $B_{\rm in}$ and $\alpha_{\rm in}$. For both expansion models ${\rm f} = f(t)$ is a function of time as given by Equation (8). For the expansion Lundquist's model, $B_{{\rm in},\phi} = B_{{\rm in},z} = B_{\rm in}$, so there are also two free parameters as for the static model. For the modified model, there is an extra free parameter; the parameters are $B_{{\rm in},\phi}$, $B_{{\rm in},z}$ and $\alpha_{\rm in}$. Notice that for all models B_z is not forced to vanish at the MC boundaries (which allows $\alpha_{\rm in}$ to be a free parameter).

Because for a fixed time t, each of the components B_ϕ and B_z have a spatial dependence as in Lundquist's model, the equations for the magnetic fluxes F_z and F_ϕ are the same as in Dasso *et al.* (2006), but now $R = R(t) = R_{\rm in} f(t)$ and $L = L(t) = L_{\rm in} f(t)$ with $R_{\rm in}$ and $L_{\rm in}$ the radius and the length, respectively, of the cylinder at time $t = t_{\rm in}$. Then, F_z and F_ϕ are, as expected, constants of motion, because the increase in $L(t)$ and $R(t)$ cancels the decay of the field components and of α. They are simply written as

$$F_z = \frac{2\pi B_{{\rm in},\phi} R_{\rm in} J_1(\alpha_{\rm in} R_{\rm in})}{\alpha_{\rm in}}, \tag{14}$$

$$F_\phi = \frac{B_{{\rm in},z}[1 - J_0(\alpha_{\rm in} R_{\rm in})]}{\alpha_{\rm in}} L_{\rm in}. \tag{15}$$

4.4. Results for the Magnetic Field

In this section we fit the MC observations with the three models described in Section 4.3. We fix the orientation to the one given in Section 3.2 ($\theta = -10°$ and $\varphi = 275°$). This allows us to test the effect of including the expansion and the decoupling of azimuthal and axial fields from the problem of finding the MC axis.

We first use the data in between "in" and "out$_3$". We use a nonlinear fitting routine to fit the models presented in Section 4.3, assuming $p = 0$, to the observations of $B_{y,\rm cloud}$

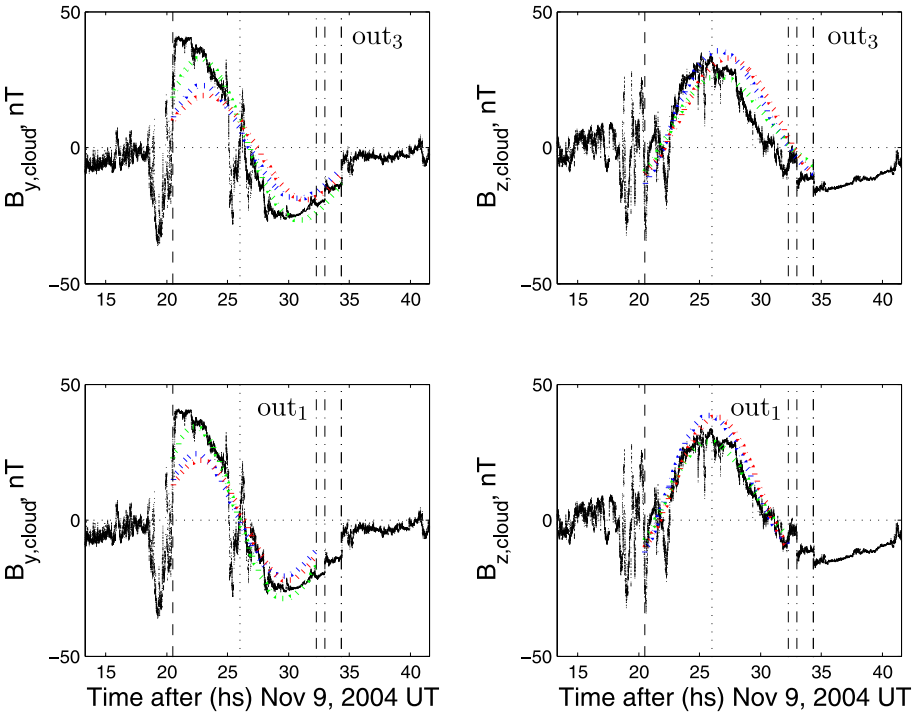

Figure 7 $B_{y,\rm cloud}$ (left panels) and $B_{z,\rm cloud}$ (right panels): observations (dots), cylindrical dynamical model (red dotted lines), cylindrical static model (blue dotted lines), and modified model (see text, green dotted lines). Upper panels show the fitting using the end time as 10 Nov. at 10:20 UT (out$_3$); lower panels use 10 Nov. at 8:15 UT (out$_1$) as the end time. Vertical lines mark the same times as in Figure 1.

(which corresponds to $\pm B_{\phi,\mathrm{cloud}}$) and $B_{z,\mathrm{cloud}}$. The static model cannot reproduce the observed asymmetry owing to the decay of the field and the shift of the position of the cloud center, because of its intrinsic symmetry (top panels of Figure 7). Both the static and expansion Lundquist's models overestimate the axial field, $B_{z,\mathrm{cloud}}$, near the cloud center and underestimate the azimuthal field, $B_{y,\mathrm{cloud}}$, near the boundaries. When the extra freedom $B_{\mathrm{in},z} \neq B_{\mathrm{in},\phi}$ is considered, the model can significantly better reproduce the observations.

A quantitative comparison of the different models is given by $\sqrt{\chi^2}$, where χ^2 is the time average of $(\mathbf{B}_{\mathrm{model}} - \mathbf{B}_{\mathrm{observations}})^2$. We find $\sqrt{\chi^2} = 14{:}16{:}19$ nT, for the modified model, and expansion and static Lundquist's models, respectively. For the three models a shift of the positions where $B_{y,\mathrm{cloud}} = 0$ and where $B_{z,\mathrm{cloud}}$ is maximum to a time later than in the observations is present (top panels of Figure 7).

We also explore the two earlier rear boundaries: "out$_1$" and "out$_2$". A significantly better fit is found with the boundary at positions "out$_1$" and "out$_2$" (with lower panels in Figure 7 showing the fitting for "out$_1$"; very similar fitted curves are obtained for "out$_2$").

A quantitative comparison between the fits is given in the form $\sqrt{\chi^2_{\mathrm{out},1}}$:$\sqrt{\chi^2_{\mathrm{out},2}}$:$\sqrt{\chi^2_{\mathrm{out},3}}$ in units of nanotesla. For the static model we obtain 16:17:19, for the expansion model 15:15:16, and for the modified model 12:12:14.

If the boundary is located at "out$_2$", the modeled cloud center corresponds now to 10 Nov. at 02:16 UT, 14 minutes later than the center given by the observations and the direct method in Section 3.3 (dotted line, 10 Nov. at 02:02 UT). For a rear boundary at "out$_1$", the modeled cloud center corresponds to 10 Nov. at 01:58 UT, only 4 minutes earlier than the value obtained using the direct method.

Let us now analyze the differences between the observations and the best model (modified Lundquist's model with boundary "out$_1$"). The model follows the observations well globally, except for the central reversal of $B_{y,\mathrm{cloud}}$ and close to the boundaries. This central reversal cannot be taken into account by the model (see Section 3.3 for an analysis of this feature). Close to the boundaries, the asymmetry of the model is not as large as the observed one; the isotropic expansion model gives $B_{y,\mathrm{out}_1}/B_{y,\mathrm{in}} = f^{-2}(t_{\mathrm{out}_1}) \approx 0.75$, whereas the observations give $\approx$0.5. Because of the crossing geometry, the data mainly reflect the radial expansion velocity. Let us now consider a refinement of this model, with radial expansion still given by $f(t)$ but axial expansion now given by $g(t) = L(t)/L_{\mathrm{in}}$ [Equation (4)]. $B_{y,\mathrm{cloud}}$ is affected both by the radial and the axial expansion. Conservation of the azimuthal flux gives $B_y(t) = B_{y,\mathrm{in}}/[f(t)g(t)]$. In the fitting of the models, we have assumed $f(t) = g(t)$, but in fact $D_{\mathrm{in}}/V_{\mathrm{c}} < T$ so that g is slightly larger than f. With $D_{\mathrm{in}}/V_{\mathrm{c}} \approx 47$ hours and $T \approx 79$ hours, we find $f_{\mathrm{out}_1} = 1.15$ and $g_{\mathrm{out}_1} = 1.25$, which gives $B_{y,\mathrm{out}_1}/B_{y,\mathrm{in}} \approx 0.69$ (rather than 0.75 with an isotropic expansion), a value closer to the observed value ($\approx$0.5) but still larger.

A spatial asymmetry between the inbound and outbound branches, which cannot be attributed to the expansion, is present in the observations (Figure 7). Indeed, the observed $B_{y,\mathrm{cloud}}$ does not have the expected decrease toward the front boundary (which is present in the model and also in the observations toward "out$_1$"; Figure 7). At the MC front the magnetic field is expected to be compressed (then, it is enhanced) by the dynamic pressure of the overtaken plasma. The interaction with the surroundings is likely to be at the origin of this extra asymmetry (on top of the expansion) between the inbound and outbound branches.

From the fitted parameters and expressions given in Equations (14) and (15), we obtain the values for the magnetic fluxes using the different models (Table 1). We assume an initial length $L_{\mathrm{in}} = 1.5$ AU as in Section 3.4. From Table 1, F_z is estimated in the range $(2.1-7.7) \times 10^{20}$ Mx, and F_ϕ in the range $(60-102) \times 10^{20}$ Mx. Fixing the end boundary

Table 1 Magnetic fluxes present in the flux rope in units of 10^{20} Mx using different fitted models or the direct method, for three backward boundaries ("out_1", "out_2", and "out_3" in Figures 1 and 2), and for an orientation given by $\theta = -10°$ and $\varphi = 275°$. For the direct method we present an average between the values obtained for the inbound and outbound branches. (F_z is not affected by including axial expansion.) The fluxes are not corrected for the flux lost by magnetic reconnection during the MC travel from the Sun (since only the direct method permits an estimation of the reconnected flux). The three models are described by the same equations but differ by the constraint set on the free parameters, so the physics involved differs [Equations (11) – (13)]. An initial length for the cloud $L_{\text{in}} = 1.5$ AU is assumed.

Model or method	"out_1"		"out_2"		"out_3"	
	F_z	F_ϕ	F_z	F_ϕ	F_z	F_ϕ
Static	7.4	60	7.7	60	7.4	60
Expanding	7.4	64	7.4	67	6.8	69
Modified	6.4	91	6.8	96	6.2	100
Direct without axial expansion	5.0	81	4.7	85	2.1	91
Direct with axial expansion	5.0	90	4.7	95	2.1	102

on 10 Nov. at 10:00 UT (only 20 minutes earlier than the boundary "out_3"), and using the static classical Lundquist's model, Longcope *et al.* (2007) reported $F_z = 7.2 \times 10^{20}$ Mx and $F_\phi/L = 41 \times 10^{20}$ Mx/AU (thus $F_\phi = 62 \times 10^{20}$ Mx, for a cloud length of $L = 1.5$ AU, as assumed here). These values, as expected, are very close to our present results with the static model and boundary "out_3". Our present results show that the expansion slightly affects the computed fluxes (and has a greater effect on F_ϕ), whereas decoupling the fits of $B_{y,\text{cloud}}$ and $B_{z,\text{cloud}}$ has the largest effect. For rear boundaries "out_1" and "out_2", the estimations of both fluxes using the modified Lundquist's model are in close agreement with the results of the direct method that consider an axial expansion; in particular this agreement is much better for F_ϕ. For the rear boundary "out_3", the value of F_z obtained from the direct method is lower than the one from the modified Lundquist's model owing to the significantly negative value of $B_{z,\text{cloud}}$ beyond "out_2" (see Figure 2); this contributes to a decrease in F_z when integrating the circular cloud section between "out_2" and "out_3". As discussed in Section 3.2, we believe that the rear boundary of the cloud should be between "out_1" and "out_2".

5. Summary and Conclusions

The ICME of 9 – 11 Nov., 2004, was a complex event with a large expansion and a strong magnetic field in the front decreasing monotonically (almost linearly) with time. Earlier analysis concluded that two magnetic clouds (MCs) were located inside this ICME (http://lepmfi.gsfc.nasa.gov/mfi/mag_cloud_S1.html). Later studies concluded that only one MC was present (Qiu *et al.*, 2007; Longcope *et al.*, 2007; Harra *et al.*, 2007). We confirm this latter result and determine the precise orientation and boundaries of the flux rope using several methods. We also find clues about the interaction of this MC with its surroundings.

To facilitate the understanding of the physics involved in the MC it is useful to transform the data to the local MC frame where the axial and azimuthal components of the magnetic field are decoupled. A classical method to determine the MC axis is the minimum variance method, which takes into account the different spatial behavior of the magnetic field components to find the flux rope orientation. We minimize the effect of the strong expansion, which implies a decreasing field magnitude with time, normalizing the field at each data

point. This gives a range of possible orientations (typically with a precision of the order of $\pm 20°$).

The determination of the orientation of the flux rope axis is improved by using the direct method. This method is based on two main points: (1) the flux rope is topologically distinct from its surroundings, so it should generically be bounded by a discontinuity of the magnetic field components (presence of a current sheet), and (2) the same amount of azimuthal magnetic flux should be present in the inbound and outbound branches of the cloud. For the cloud of 9 – 10 Nov. 2004 the frontal discontinuity is well defined, whereas three rear discontinuities are present ("out_1", "out_2", and "out_3"). They are separated by about 2 hours compared to a MC duration of about 14 hours. The azimuthal flux relates the frontal discontinuity to two discontinuities at the rear using two different hypotheses for the axial evolution: an expansion comparable to the radial one gives a rear discontinuity at "out_2", and a negligible axial expansion gives a rear discontinuity at "out_3". However, because the second case implies a reversal of the axial field at the rear of the MC, we conclude that the first discontinuity ("out_2") is associated with the frontal discontinuity. This defines precisely the extension, as well as the orientation angle θ (within $\pm 5°$, $\theta = 10 \pm 5°$) of the flux rope.

Fitting a model to the data is another approach to understand the observed magnetic structure. We have used three models that are based on Lundquist's solution. The first one is the classical static solution. The second one includes a self-similar expansion with the same rate in the axial and radial directions. Finally, the third one also includes an isotropic expansion and decouples the fit of the azimuthal and axial field components to take into account the observed stronger azimuthal component (a possible signature of a flat cross section). The expansion rate is obtained by fitting the model to the observed plasma velocity. The best fits to the data are obtained when the first and second discontinuities (labeled "out_1" and "out_2") are used, in agreement with the results obtained with the direct method.

Comparing the results of the fitted models with the direct method, using boundaries "out_1" and "out_2", we find that the axial and azimuthal fluxes are in the ranges $(4.7 – 7.7) \times 10^{20}$ Mx and $(60 – 96) \times 10^{20}$ Mx, respectively. The main limitation on the axial flux measurements is the unknown shape of the cross section. For the azimuthal flux, it is important to consider the axial expansion. Here the limitations are different: The shape of the cross section is not important, and the main limitation is the distribution of the flux along the MC axis. Finally, we confirm that the azimuthal flux is one order of magnitude larger than the axial flux.

After the large and coherent rotation of **B**, some typical MC characteristics are still present: a low level of fluctuations, strong expansion (observed in the decay of V and B), a magnetic field intensity higher than typical solar wind values, and low β_{p}. This is evidence that the MC extends farther in the back of the flux rope. Part of this back (from "out_3" to "back" in Figures 1 and 2) shows a coherent behavior of $B_{y,\text{cloud}}$, which we interpret as the signature of an originally larger flux rope that was partially reconnected in its front near the Sun, with the consequent flux removal.

Reconnection of the cloud field with the overtaken solar wind field is another source of underestimation of the original magnetic flux that was launched from the Sun. We have found that $\sim$17% (with 30% as an upper bound) of the azimuthal flux was lost in the front of the MC during its travel from the Sun; this is much less than in the 18 – 20 Oct. 1995, MC, where it was estimated to be about 57% (Dasso *et al.*, 2006). Another difference between the MCs is that the 9 – 10 Nov. MC has a back part moving at a speed significantly lower (by $\approx$200 km s^{-1}) than the flux rope (whereas the 18 – 20 Oct. MC was overtaken by a fast stream). Then, the reconnected field progressively forms an extended region in the back of the flux rope (with a weaker magnitude but still with a smooth spatial variation). From

the extension and velocity difference of this region with the flux rope, we have estimated that reconnection started close to the Sun, possibly between the erupting twisted flux tube (giving the flux rope) and the overlying arcade of active region 10696. Part of the arcade field is probably present in front of the MC, with a nearly antiparallel direction and a significant velocity difference ($\approx$40 km s^{-1}), indicating that magnetic reconnection is not so efficient in the interplanetary space.

Reconnection in front of the MC has several observational consequences, as follows: First, it introduces an asymmetry in the observed magnetic field. The remaining part of the flux rope is observed first, followed by an extended tail of weaker magnetic field (which is reorientated since it has changed its connectivity). When this process is dominantly at work, this implies the presence of a closed flux rope at the beginning of the ICME. Second, depending on the solar launch direction, the spacecraft could cross the flux rope or its laterally extended back part. In this last case, one would detect some characteristics of the MC (such as a coherent field and low β values), but without the coherent rotation of the field. Such a crossing would be classified as an ICME (without an MC). An example of such observations with the two *Helios* spacecraft is analyzed by Cane, Richardson, and Wibberenz (1997) and another example using the ACE spacecraft is analyzed by Foullon *et al.* (2007).

Finally, the back flux connected to the solar wind field makes the moving magnetic structure larger in the transverse direction (orthogonal to the global motion). From its mixed origin the back region is expected to move at a speed intermediate between the MC and the solar wind speed, as observed in the MC analyzed here. Then, with a significantly larger velocity than the surrounding medium, the back region is expected to have an effect on the frontal shock surrounding the ICME. A larger transverse scale implies a forward shock at a larger distance in front of the MC than the distance deduced by its flux rope transverse size (Farris and Russell, 1994). Such a large distance has so far been interpreted as a flat flux rope (Russell and Mulligan, 2002). The consequence of reconnection in the front of the MC is an alternative and/or complementary explanation that requires numerical simulations to be quantified.

The results obtained show the potential of combining several methods of analysis — minimum variance, the direct method, and a fit to the data. This analysis will be done for other MCs to derive the variety of possible physical scenarios and also to improve our understanding of MCs and ICMEs.

Acknowledgements The authors are grateful to L.K. Harra for organizing the Sun – Earth Connection workshop at MSSL from which this contribution is an outcome. This workshop was possible thanks to a Phillip Leverhulm Prize. S.D. would like to thank N.U. Crooker and H. Elliott for helpful discussions. This research has made use of NASA's Space Physics Data Facility (SPDF). C.H.M. and P.D. acknowledge financial support from CNRS (France) and CONICET (Argentina) through their cooperative science program (No. 20326). This work was partially supported by the Argentinean grants UBACyT X329, PIP 6220 (CONICET), and PICTs 03-14163, 03-12187, and 03-33370 (ANPCyT). S.D. and C.H.M. are members of the Carrera del Investigador Científico, CONICET. M.S.N. is a fellow of CONICET. The authors would like to thank the referee, whose constructive criticisms helped us to improve this paper.

References

Attrill, G., Nakwacki, M.S., Harra, L.K., van Driel-Gesztelyi, L., Mandrini, C.H., Dasso, S., Wang, J.: 2006, *Solar Phys.* **238**, 117.

Berdichevsky, D.B., Lepping, R.P., Farrugia, C.J.: 2003, *Phys. Rev. E* **67**(3), 036405.

Bothmer, V., Schwenn, R.: 1998, *Ann. Geophys.* **16**, 1.

Burlaga, L.F.: 1988, *J. Geophys. Res.* **93**, 7217.

Burlaga, L.F.: 1995, *Interplanetary Magnetohydrodynamics*, Oxford University Press, New York.

Cane, H.V., Richardson, I.G., Wibberenz, G.: 1997, *J. Geophys. Res.* **102**, 7075.
Cid, C., Hidalgo, M.A., Nieves-Chinchilla, T., Sequeiros, J., Viñas, A.F.: 2002, *Solar Phys.* **207**, 187.
Dasso, S., Mandrini, C.H., Démoulin, P., Farrugia, C.J.: 2003, *J. Geophys. Res.* **108**(A10), 1362.
Dasso, S., Gulisano, A.M., Mandrini, C.H., Démoulin, P.: 2005a, *Adv. Space Res.* **35**, 2172.
Dasso, S., Mandrini, C.H., Démoulin, P., Luoni, M.L., Gulisano, A.M.: 2005b, *Adv. Space Res.* **35**, 711.
Dasso, S., Mandrini, C.H., Démoulin, P., Luoni, M.L.: 2006, *Astron. Astrophys.* **455**, 349.
Farris, M.H., Russell, C.T.: 1994, *J. Geophys. Res.* **99**, 17681.
Farrugia, C.J., Osherovich, V.A., Burlaga, L.F.: 1997, *Ann. Geophys.* **28**, 152.
Farrugia, C.J., Burlaga, L.F., Osherovich, V.A., Richardson, I.G., Freeman, M.P., Lepping, R.P., Lazarus, A.J.: 1993, *J. Geophys. Res.* **98**, 7621.
Farrugia, C.J., *et al.*: 1999, *AIP Conf. Proc.* **471**, 745.
Farrugia, C.J., *et al.*: 2001, *Adv. Space Res.* **28**, 759.
Foullon, C., Owen, C.J., Dasso, S, Green, L.M., Dandouras, I., Elliott, H.A., Fazakerley, A.N., Bogdanova, Y.V., Crooker, N.N.: 2007, *Solar Phys.*, DOI: 10.1007/s11207-007-0355-y.
Gibson, S.E., Fan, Y., Mandrini, C., Fisher, G., Démoulin, P.: 2004, *Astrophys. J.* **617**, 600.
Goldstein, H.: 1983, In: *Solar Wind Conference*, 731.
Gosling, J.T., Skoug, R.M., McComas, D.J., Smith, C.W.: 2005, *J. Geophys. Res.* **110**, 1107.
Gulisano, A.M., Dasso, S., Mandrini, C.H., Démoulin, P.: 2005, *J. Atmos. Solar Terr. Phys.* **67**, 1761.
Harra, L.K., Crooker, N.N., Mandrini, C.H., van Driel-Gesztelyi, L., Dasso, S., Wang, Y.X., Elliott, H., Attrill, G.D., Jackson, B.V., Bisi, M.B.: 2007, *Solar Phys.*, DOI: 10.1007/s11207-007-9002-x.
Hidalgo, M.A.: 2003, *J. Geophys. Res.* **108**(A8), 1320.
Hidalgo, M.A., Cid, C., Vinas, A.F., Sequeiros, J.: 2002, *J. Geophys. Res.* **107**(A1), 1002.
Hu, Q., Sonnerup, B.U.Ö.: 2001, *Geophys. Res. Lett.* **28**, 467.
Klein, L.W., Burlaga, L.F.: 1982, *J. Geophys. Res.* **87**(A16), 613.
Lepping, R.P., Burlaga, L.F., Jones, J.A.: 1990, *J. Geophys. Res.* **95**, 11957.
Lepping, R.P., *et al.*: 1995, *Space Sci. Rev.* **71**, 207.
Lepping, R.P., Berdichevsky, D.B., Szabo, A., Arqueros, C., Lazarus, A.J.: 2003, *Solar Phys.* **212**, 425.
Longcope, D., Beveridge, C., Qiu, J., Ravindra, B., Barnes, G., Dasso, S.: 2007, *Solar Phys.*, DOI: 10.1007/s11207-007-0330-7.
Lundquist, S.: 1950, *Ark. Fys.* **2**, 361.
Lynch, B.J., Zurbuchen, T.H., Fisk, L.A., Antiochos, S.K.: 2003, *J. Geophys. Res.* **108**(A6), 1239.
Mandrini, C.H., Pohjolainen, S., Dasso, S., Green, L.M., Démoulin, P., van Driel-Gesztelyi, L., Copperwheat, C., Foley, C.: 2005, *Astron. Astrophys.* **434**, 725.
Mandrini, C.H., Nakwacki, M.S., Attrill, G., van Driel-Gesztelyi, L., Démoulin, P., Dasso, S., Elliott, H.: 2007, *Solar Phys.*, in press.
Morales, L.F., Dasso, S., Gómez, D.O.: 2005, *J. Geophys. Res.* **110**, 4204.
Mulligan, T., *et al.*: 1999, *AIP Conf. Proc.* **471**, 689.
Nakwacki, M.S., Dasso, S., Mandrini, C.H., Démoulin, P.: 2005, In: *Proceedings Solar Wind 11 – SOHO 16*, *ESA SP-592*, ESA, Noordwijk, 629.
Nakwacki, M.S., Dasso, S., Mandrini, C.H., Démoulin, P.: 2007, *J. Atmos. Solar Terr. Phys.*, submitted.
Ogilvie, K.W., *et al.*: 1995, *Space Sci. Rev.* **71**, 55.
Osherovich, V.A., Farrugia, C.J., Burlaga, L.F.: 1993, *J. Geophys. Res.* **98**(A8), 13225.
Qiu, J., Hu, Q., Howard, T.A., Yurchyshyn, V.B.: 2007, *Astrophys. J.* **659**, 758.
Riley, P., *et al.*: 2004, *J. Atmos. Solar Terr. Phys.* **66**, 1321.
Russell, C.T., Mulligan, T.: 2002, *Adv. Space Res.* **29**, 301.
Russell, C.T., Shinde, A.A.: 2005, *Solar Phys.* **229**, 323.
Schmidt, J.M., Cargill, P.J.: 2003, *J. Geophys. Res.* **108**, 5.
Shimazu, H., Vandas, M.: 2002, *Earth Planets Space* **54**, 783.
Sonnerup, B.U., Cahill, L.J.: 1967, *J. Geophys. Res.* **72**, 171.
Török, T., Kliem, B.: 2005, *Astrophys. J. Lett.* **630**, L97.
Vandas, M., Romashets, E.P.: 2002, In: *Solar Variability: From Core to Outer Frontiers*, *ESA SP-506*, ESA, Noordwijk, 217.
Vandas, M., Romashets, E.P.: 2003, *Astron. Astrophys.* **398**, 801.
Vršnak, B., Gopalswamy, N.: 2002, *J. Geophys. Res.* **107**(A2), 1019.
Williams, D.R., Török, T., Démoulin, P., van Driel-Gesztelyi, L., Kliem, B.: 2005, *Astrophys. J. Lett.* **628**, L163.
Wimmer-Schweingruber, R.F., *et al.*: 2006, *Space Sci. Rev.* **123**, 177.